Zhuqian Zhang
School of Mechanical Electronic and Control Engineering,
Beijing Jiaotong University,
Beijing, P.R.C.

Xia Wang[1]
Department of Mechanical Engineering,
Oakland University,
Rochester, MI
e-mail: wang@oakland.edu

Xinxin Zhang
School of Mechanical Engineering,
University of Science and Technology Beijing,
Beijing, P.R.C.

Li Jia
School of Mechanical Electronic and Control Engineering,
Beijing Jiaotong University,
Beijing, P.R.C.

Optimizing the Performance of a Single PEM Fuel Cell

A three-dimensional steady-state electrochemical mathematical model is developed where the mass, fluid, and thermal transport processes are considered, as well as the electrochemical reaction phenomena. The influences of the parameters of interest, which include porosity, permeability, and the thickness of the gas diffusion layer, and the inlet gas stoichiometric ratio on the performance of fuel cells are identified. By applying the Powell algorithm, the optimum values of multiple parameters are obtained while optimizing the potential of the electrolyte phase at the membrane/cathode interface at a typical value of the cell voltage. Compared with the reference case, the optimized results, such as the oxygen mole fraction and the local current density distribution, provide useful information for a better design of fuel cells. [DOI: 10.1115/1.2889051]

1 Introduction

Porous electrodes in polymer electrolyte membrane (PEM) fuel cells play an important role in transition with the minimum voltage losses, from the channel-land structure of the flow field to the active area of the electrodes, to ensure a homogeneous and efficient mass transport over the whole active area of the cell [1]. Electrochemical behavior of porous electrodes in PEM fuel cells is influenced by several factors, including the inner structure such as porosity and permeability and the thickness of the gas diffusion layer (GDL). It is difficult to evaluate the influence of a single parameter while other properties are kept constant. For example, the change of GDL permeability and the gas flow rate may affect the channel pressure drop to various degrees [2]. It is, therefore, important to analyze the effects of various electrode parameters on the performance of PEM fuel cells.

Numerical simulation is a very useful tool to study the transport and electrochemical reaction phenomena, which can also be used to optimize the performance of fuel cells. Over the last decades, several fuel cell models have been developed. Bernardi [3] and Springer et al. [4] developed one-dimensional polymer electrolyte (PEM) fuel cell models, which provided a fundamental framework for the multidimensional models that followed. Later on, two-dimensional models [5–8] were developed, which considered the changes both across the membrane and in the direction of the bulk flow. A good example can be seen from the research by Yi and Nguyen [7], where the two-dimensional flow approach was used to investigate the multicomponent transport in porous electrodes of a PEM fuel cell with the interdigitated gas distributors. The model proposed by Yi and Nguyen [7] predicted the current density generated at the membrane/electrode interface as a function of various operating conditions and design parameters. It was shown that the average current density generated at the cathode increased with the higher gas flow rate, thinner electrode, and narrower shoulder between the inlet and outlet channels of the interdigitated gas distributor. Most recently, several three-dimensional models [9,10] have been developed for a more accurate prediction of the fuel cell performance, especially those using the computational fluid dynamics (CFD) approaches [11–15].

Some experiments have been performed to investigate PEM fuel cells [16–21]. However, the optimization by experiments is time consuming and expensive compared to the numerical optimization, which can yield the global optimization since many parameters can be simultaneously varied. Williams et al. [19] experimentally investigated the performance of PEM fuel cells with no external humidification by optimizing the operating cell temperature and the inlet gas stoichiometric ratio. It was found that to obtain the maximum cell performance, the optimal cathode stoichiometric ratio was corresponding to different operating temperatures while the anode stoichiometric ratio was maintained constant. Their work also showed that it was possible to run a fuel cell with no external humidification as long as the critical parameters were optimized. Lee et al. [20] investigated the effects of the gas diffusion layer thickness by the numerical simulation and concluded that an intermediate thickness enhanced the electrodes' performance best. Grujicic and Chittajallu [21] performed a steady-state, two-dimensional electrochemical model with a nonlinear constrained optimization algorithm to optimize the cathode geometry. The optimal cathode design was found to be associated with the cathode geometrical parameters, such as the thickness and length per shoulder of the interdigitated air distributor.

This work will focus on the numerical optimization of gas diffusion layer with respect to the electrode design parameters, such as porosity, permeability, and the thickness of the GDL and the inlet gas stoichiometric ratio. A three-dimensional steady-state electrochemical mathematical model of the unit cell, which considers the mass, fluid, and thermal transport processes as well as the electrochemical reaction, is solved by coupling with the Powell optimization algorithm. In addition, the influence of the electrode parameters on the performance of fuel cells is analyzed and the corresponding optimal values are obtained.

2 Mathematical Models

2.1 Computational Models. The computational domain of the whole unit cell, as shown in Fig. 1, consists of nine different regions along the Z axis from cathode to anode: the cathode current collector, the cathode channel, the cathode diffusion layer, the

Manuscript received June 4, 2006; final manuscript received August 24, 2007; published online May 23, 2008. Review conducted by Ken Reifsnider.

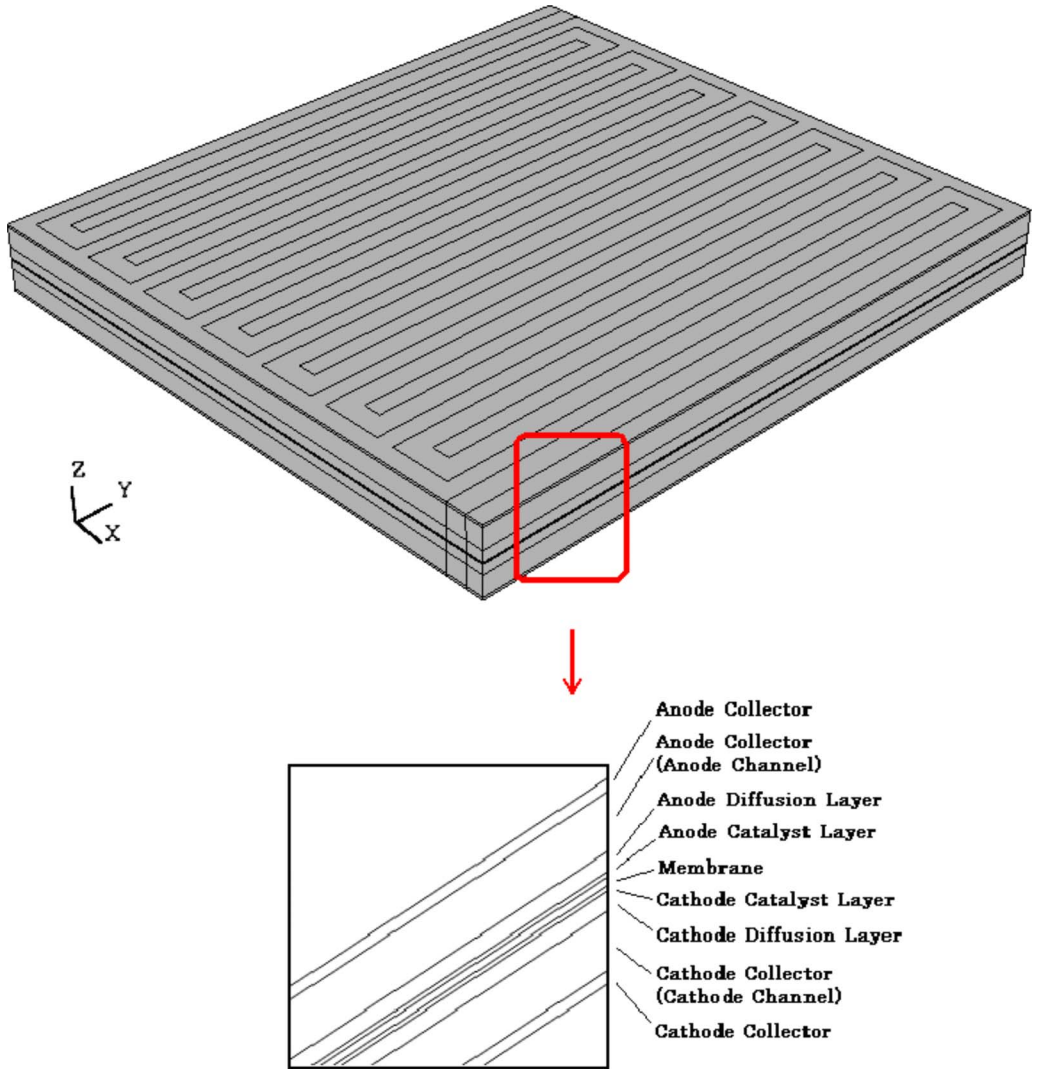

Fig. 1 Physical model of PEM fuel cell

cathode catalyst layer, the proton exchange membrane, the anode catalyst layer, the anode diffusion layer, the anode channel, and the anode current collector.

The flow field used in the current model is a single-serpentine flow pattern with a rectangular channel of 0.84 mm in width and 0.81 mm in depth, and 14 pieces of 180 deg turns (15 passages in total). The total length of a single channel is 38.1 cm and the total active area is 6.25 cm^2. The anode and cathode flow fields are in a counterflow orientation and the reactants are pure hydrogen and air. This flow field is chosen to be the same as the one shown in Ref. [19]. The details of the flow fields are summarized in Table 1. Table 1 also lists other physical properties used by the current model.

The current model is based on the following assumptions: The cell operates under the steady-state condition; the reactants are treated as the ideal gas; an incompressible laminar flow is assumed everywhere in the channels; an isotropic porous medium exists in the diffusion layers, catalyst layers, and the membrane; and the gas within the electrodes exists as a continuous phase, so that Darcy's law is applied.

The governing equations in the vector form are shown as follows: Continuity,

$$\nabla \cdot (\varepsilon \rho \mathbf{U}) = S_m \tag{1}$$

Momentum conservation,

Table 1 Physical parameters and properties

Channel thickness	0.81 mm
Cathode diffusion layer thickness	0.373 mm
Anode diffusion layer thickness	0.429 mm
Catalyst layer thickness	0.02 mm
Membrane thickness	0.026 mm
Membrane porosity	0.28
Catalyst layer porosity	0.4
Diffusion layer porosity	0.4
Inlet nitrogen/oxygen mole ration	0.78/0.205
Cell operating temperature	70°C
Air-side inlet pressure/fuel-side inlet pressure	1/1 atm
Membrane permeability	1×10^{-18} m^2
Catalyst layer permeability	1×10^{-11} m^2
Diffusion layer permeability	1×10^{-11} m^2
O_2 stoichiometric ratio	1.5, 2, 2.5, 3, 4
H_2 stoichiometric ratio	1.3, 3
Relative humidity of inlet fuel/air	27%/1.5%
Reference exchange current density of anode	4.72×10^9 A/m^3
Reference exchange current density of cathode	5.376×10^6 A/m^3
Cathode transfer coefficient	0.75
Anode transfer coefficient	0.25

Table 2 Source terms in different regions of PEM fuel cell

Channels	Diffusion layers	Catalyst layers	Membrane
$S_m=0$	$S_m=0$	$S_m=\frac{M_i}{nF}i$	$S_m=0$
$S_u=0$	$S_u=-\frac{\mu_{\text{eff}}}{\kappa_p}\varepsilon^2\mathbf{U}$	$S_u=-\frac{\mu_{\text{eff}}}{k_p}\varepsilon\mathbf{U}+\frac{k_\varphi}{k_p}z_f c_f F\nabla\Phi_e$	$S_u=-\frac{\mu_{\text{eff}}}{k_p}\varepsilon\mathbf{U}+\frac{k_\varphi}{k_p}z_f c_f F\nabla\Phi_e$
$S_T=0$	$S_T=\frac{i_s^2}{\sigma_{s,eff}}$	$S_T=\frac{i^2}{\sigma_{\text{eff}}}+\left[\frac{T(-\Delta S)}{nF}+\eta_{act}\right]i$	$S_T=\frac{i_e^2}{\sigma_{e,eff}}$
$S_i=0$	$S_i=0$	$S_i=\frac{M_i}{nF}i$	$S_i=0$
$S_{\phi_e}=0$	$S_{\phi_e}=0$	$S_{\phi_e}=i_0$	$S_{\phi_e}=0$
$S_{\phi_s}=0$	$S_{\phi_s}=0$	$S_{\phi_s}=-i_0$	$S_{\phi_s}=0$

$$\nabla\cdot(\varepsilon\rho\mathbf{U}\mathbf{U})=-\varepsilon\nabla p+\nabla\cdot(\varepsilon\mu_{\text{eff}}\nabla\mathbf{U})+S_u \tag{2}$$

Energy conservation,

$$\nabla\cdot(\lambda_{\text{eff}}\nabla T)=\nabla\cdot(\varepsilon\rho C_p\mathbf{U}T)+S_T \tag{3}$$

Species conservation,

$$\nabla\cdot(\varepsilon\mathbf{U}Y_i)=\nabla\cdot(D_{i,\text{eff}}\nabla Y_i)+S_i \tag{4}$$

Potential conservation,

$$\nabla\cdot(\sigma_{e,\text{eff}}\nabla\Phi_e)=S_{\phi_e} \tag{5}$$

$$\nabla\cdot(\sigma_{s,\text{eff}}\nabla\Phi_s)=S_{\phi_s} \tag{6}$$

where $\mathbf{U}$ is the fluid velocity vector; Y_i the mole fraction of species i; T the fluid temperature; Φ_e and Φ_s represent the electrolyte phase and the solid phase potential of electrodes, respectively; ε the porosity of electrodes; μ_{eff} the effective viscosity of the fluid; λ_{eff} the effective heat conductivity; $D_{i,\text{eff}}$ the effective mass diffusivity of species i; and $\sigma_{e,\text{eff}}$ and $\sigma_{s,\text{eff}}$ are the ionic conductivity of electrolyte phase and the electronic conductivity of solid phase, respectively. The source terms S_m, S_u, S_T, S_i, S_{ϕ_e}, and S_{ϕ_s} are shown in Table 2 for different regions.

It is sufficient to solve the dc conduction equation (conservation of current) instead of the electrostatic equation (conservation of charge) based on the assumption of electroneutrality. Therefore, the DC conduction equation is given as

$$\nabla\cdot\mathbf{i}=0 \tag{7}$$

where $\mathbf{i}$ is the total current density vector. In the active catalyst layers region, one part of the current will flow through the substrate solid (or electronic), and the other through the electrolyte fluid (or ionic). Thus,

$$\mathbf{i}=\mathbf{i}_e+\mathbf{i}_s \tag{8}$$

and

$$-\nabla\cdot\mathbf{i}_e=-\nabla\cdot\mathbf{i}_s=i_0 \tag{9}$$

$$-\nabla\cdot(-\sigma_{e,\text{eff}}\nabla\Phi_e)=\nabla\cdot(-\sigma_{s,\text{eff}}\nabla\Phi_s)=i_0 \tag{10}$$

These two current components are completely independent. The only way that they can interact with each other is through electrochemical reactions, where electrons are either transferred to the solid from the pore phase or vice versa. The transfer current i_0 is a measure of the electrochemical reaction rate. In general, it is typically expressed by the Butler–Volmer equation

$$i_0=i_{0,\text{ref}}\left\{\exp\left[\frac{\alpha_a nF}{RT}\eta\right]-\exp\left[\frac{-\alpha_c nF}{RT}\eta\right]\right\} \tag{11}$$

where η is the overpotential, where $\eta=(\Phi_s-\Phi_e)-E_{ocv}$; F is the Faraday constant; α_a and α_c represent the experimental anodic and cathodic Tafel constants, respectively; and R is the gas constant.

The numerical domain used here is a full single cell geometry

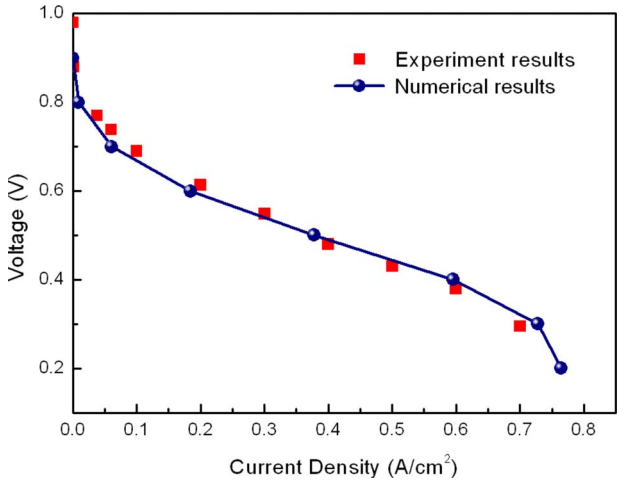

Fig. 2 Comparison between the numerical prediction and experimental data [19]

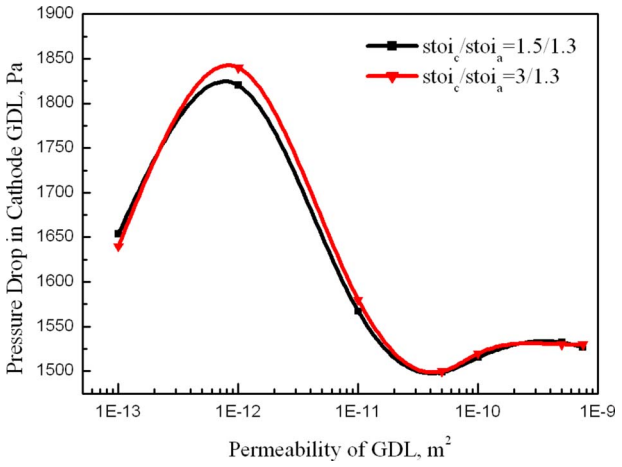

Fig. 3 The pressure drop in the GDL as a function of permeability and the gas inlet stoichiometric ratio

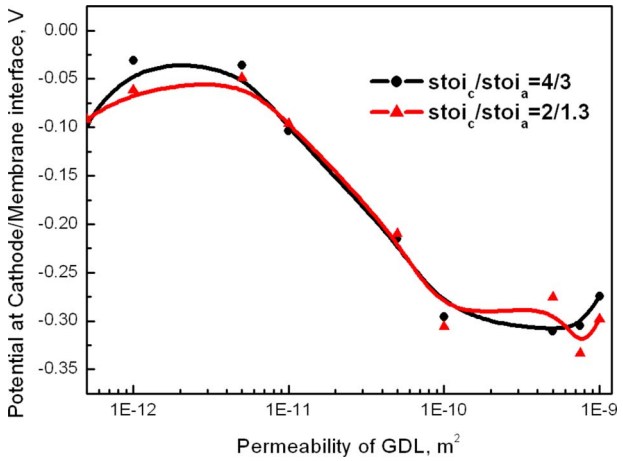

Fig. 4 The electrolyte fluid phase potential at the cathode/membrane interface as a function of permeability and the gas inlet stoichiometric ratio

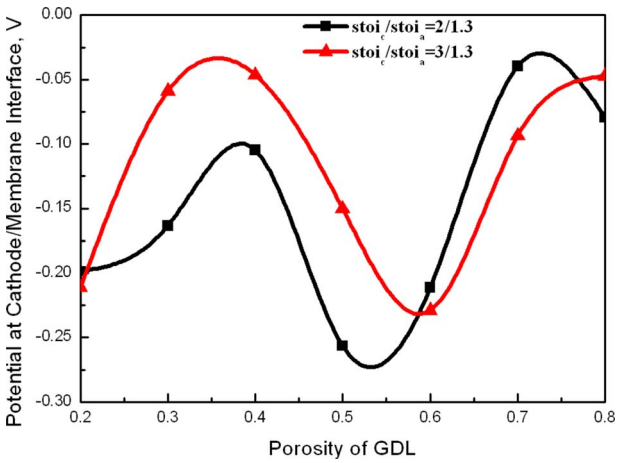

Fig. 6 The electrolyte fluid phase potential at the cathode/membrane interface as a function of porosity and the gas inlet stoichiometric ratio

region. At the entrances of the gas channels, the pressure and mole fraction of each species are specified in Table 1. The hydrogen and air flow rate in the inlet was calculated based on the average current density of 1 A/cm^2 and the gas inlet stoichiometric ratio. Pressure boundary conditions are prescribed at the outlets. Both the velocity and mass fraction distributions are assumed to be fully developed in the gas channels. Zero flux boundary conditions are applied to the other external surfaces of the domain.

The conservation equations, Eqs. (1)–(6), were discretized using a finite volume method [22] and solved iteratively using a commercial CFD code CFD-ACE+, developed by the ESI CFD Incorporation. The polarization curve, shown in Fig. 2, displays a strong agreement between the predicted results and the experiment data published in literatures [19]. The maximum difference percentage between the numerical and experimental result is below 4.76%. This might be due to the fact that the contact electrical resistance within components is not taken into account in the numerical model despite the experimental uncertainty.

2.2 Simulation Results: Parametric Study. In this section, the effects of electrode parameters and stoichometric ratio on the pressure drop across the GDL will be studied. The cell is kept at a constant potential of 0.6 V and at various values of the cathode

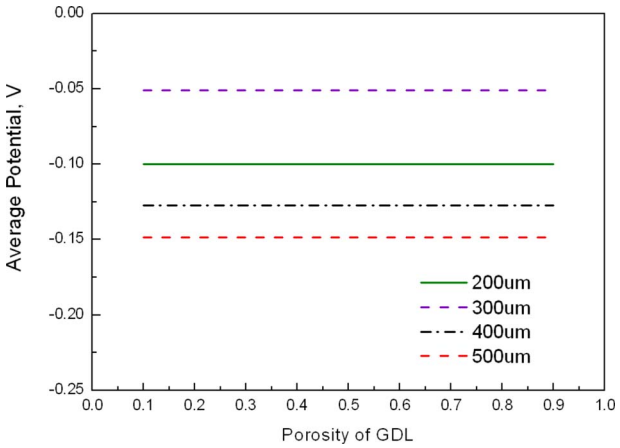

Fig. 7 Average electrolyte fluid phase potential at the cathode/membrane interface as a function of porosity and the GDL thickness

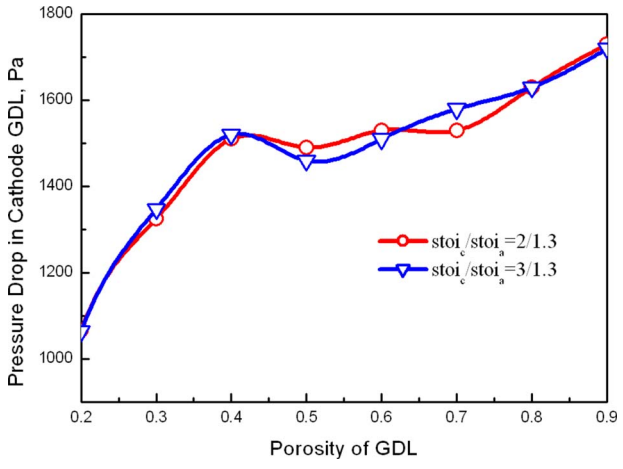

Fig. 5 The pressure drop in the GDL as a function of porosity and the gas inlet stoichiometric ratio

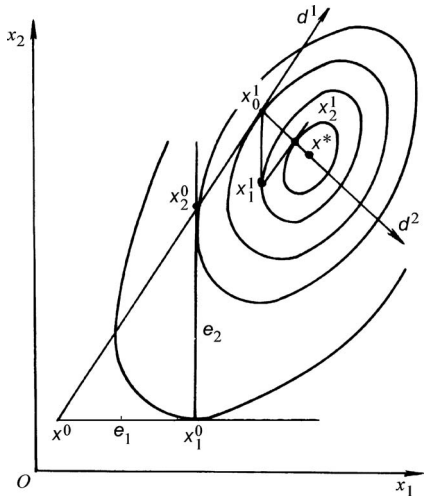

Fig. 8 Searching scheme of the Powell method

Table 3 Initial parameter settings for the Powell algorithm

Cathode GDL permeability, $x(1)$	$1E-11$ m^2
Anode GDL permeability, $x(2)$	$1E-11$ m^2
Cathode GDL porosity, $x(3)$	0.4
Anode GDL porosity, $x(4)$	0.4
Cathode GDL thickness, $x(5)$	0.373 mm
Anode GDL thickness, $x(6)$	0.429 mm
Cathode inlet gas stoichiometric ratio, $x(7)$	2
Anode inlet gas stoichiometric ratio, $x(8)$	1.3

Table 4 Optimized values obtained from the Powell algorithm

Cathode GDL permeability, $x(1)$	$5.40E-12$ m^2
Anode GDL permeability, $x(2)$	$6.48E-12$ m^2
Cathode GDL porosity, $x(3)$	0.527
Anode GDL porosity, $x(4)$	0.735
Cathode GDL thickness, $x(5)$	0.437 mm
Anode GDL thickness, $x(6)$	0.404 mm
Cathode inlet gas stoichiometric ratio, $x(7)$	3
Anode inlet gas stoichiometric ratio, $x(8)$	1.3

stoichiometric ratio between 1.5 and 4, and at two different values of the anode stoichiometric ratio (1.3 and 3). The cell is operating at pressure of 1 atm pressure and temperature of 70°C.

Serpentine flow fields result in a very long channel with relatively small cross area. Therefore, a large pressure drop occurs across the GDL, which is the main driving force for the gas to pass through the GDL. This behavior is described by Darcy's law [23] given as

$$\upsilon = \frac{\kappa}{\varepsilon\mu}\frac{\Delta P}{l} \tag{12}$$

where υ is the stoichiometric flow rate, κ the permeability of the GDL, ΔP the pressure drop, l the thickness of the GDL, and μ the dynamic viscosity of fluids.

The reactant gas flow rate can be described by a stoichiometric flow ratio,ζ, defined as the actual amount of the reactant gas feed divided by the amount required by the electrochemical reaction. Accordingly, the gas inlet stoichiometric flow rate can be evaluated as [24]

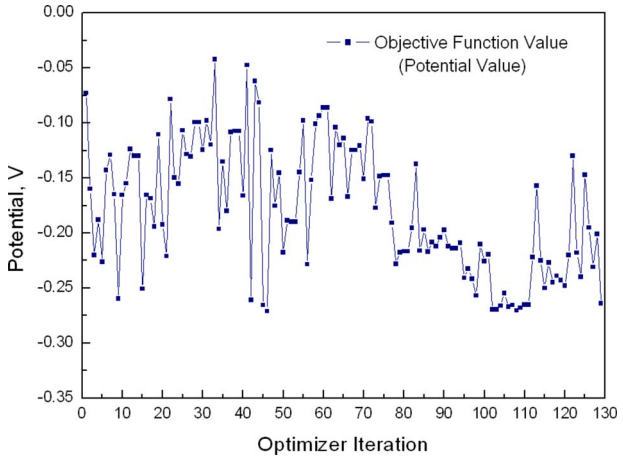

Fig. 9 Objective functions with iteration

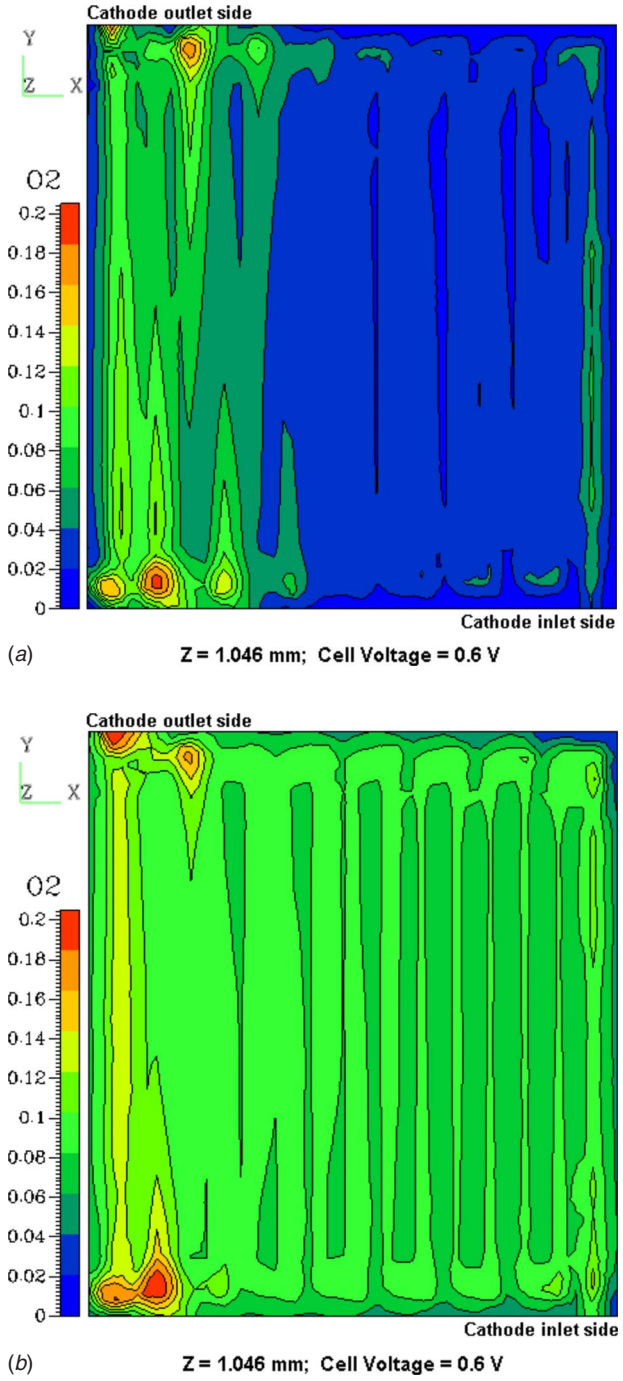

Fig. 10 Contours of oxygen mole fraction in the GDL for (*a*) before and (*b*) after optimization

$$\upsilon = \zeta\frac{i_{\text{av}}}{nF}A_m\frac{1}{x_{i,\text{in}}}\frac{RT_{\text{in}}}{p_{\text{in}}}\frac{1}{A_{\text{ch}}} \tag{13}$$

where A_m and A_{ch} are the active area of the membrane and the channel section, respectively;i_{av} is the average current density;T_{in}, p_{in}, and $x_{i,\text{in}}$ are the temperature, pressure, and species mole fraction at the entrance of the gas channels, respectively.

2.2.1 Effects of GDL Permeability κ and Gas Inlet Stoichiometric Ratio. The values of the GDL permeability vary greatly from 10^{-13} m^2 to 10^{-10} m^2 in the published literature. Figure 3 shows the pressure drop across the cathode GDL as a function of

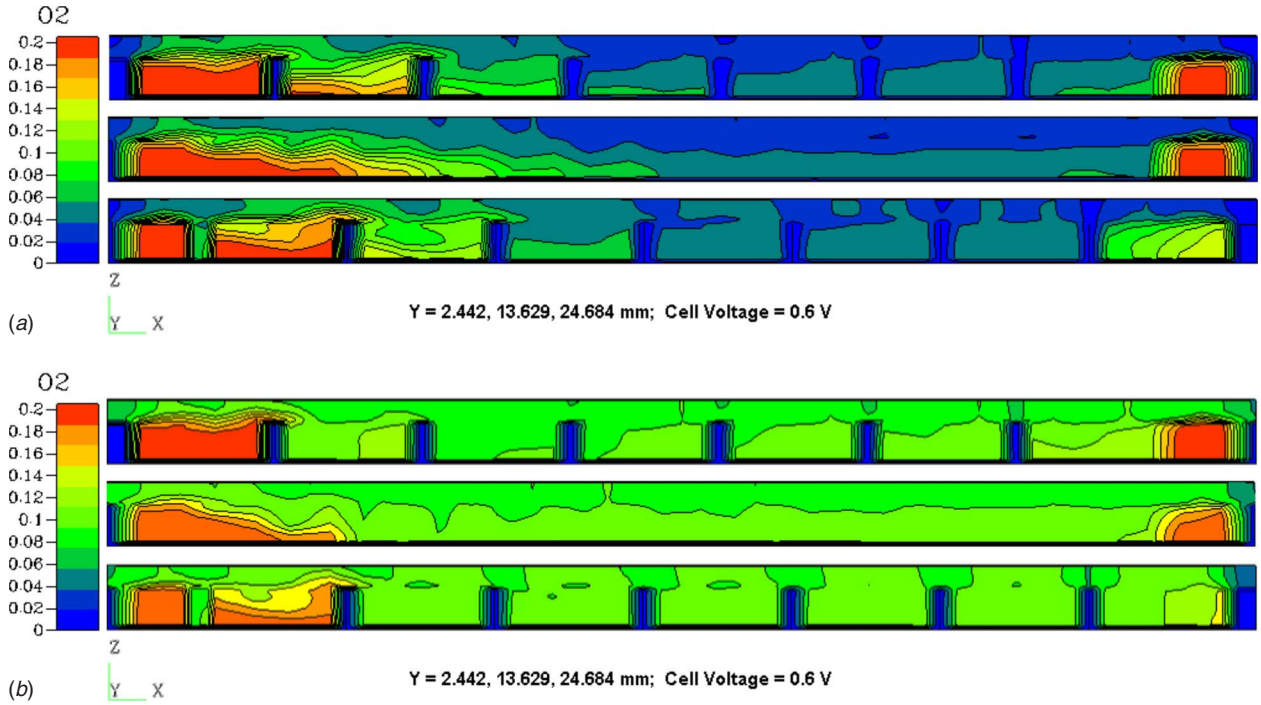

Fig. 11 Contours of oxygen mole fraction throughout the cathode thickness at three different *Y* locations (*a*) before and (*b*) after optimization

permeability and the gas inlet stoichiometric ratio.

The pressure drop reaches the maximum when the value of permeability is around $(6-10)\times 10^{-13}$ m^2 and then drops sharply until the value of permeability is approximately 2×10^{-11} m^2. The gas inlet stoichiometric ratios have a weak influence on the pressure drop in the GDL. When permeability is very small, reactants can barely diffuse through the gas diffusion layer, thus resulting in a small pressure drop. When the permeability increases, reactants will diffuse more easily to the cathode reaction side, resulting in an increase of the pressure drop. If permeability continues to increase, the concentration of water at the cathode side will increase due to the fast chemical reaction. Therefore, water vapor will diffuse back to the flow channel through the gas diffusion layer, thus resulting in a less resultant pressure drop.

Figure 4 shows the fitting curve of the electrolyte fluid phase potential at the cathode/membrane interface with different permeabilities and two cathode/anode inlet stoichiometric ratios. A higher potential at the cathode/membrane interface corresponds to a more active electrochemical reaction, which leads to an increase in the oxygen consumption. In Fig. 4, a relatively small potential occurs at lower permeability, which is due to less amount of reactant diffusion at lower permeability. At higher permeability, the potential increases at the cathode membrane/catalyst interface. These results suggest that there will be an optimum value of the GDL permeability and the stoichiometric ratio under the present operating conditions, where gases transport effectively in the GDL.

2.2.2 Effect of GDL Porosity ε and GDL Thickness. Porosity of the GDL is another sensitive parameter affecting the cell performance. A larger porosity of the GDL leads to a greater space for the diffusion, which, however, induces a higher contact resistance in the GDL. There must be an optimum porosity level for the GDL so that the fuel cell has its best performance [25].

Figures 5 and 6 display the changes of the pressure drop and the potential at the cathode/membrane interface with different values of the GDL porosities and the gas inlet stoichiometric ratios. The gas inlet stoichiometric ratio has a little effect on the pressure drop, as shown in Fig. 5. However, as the porosity increases, the pressure drop in cathode GDL increases sharply (especially below 0.4 of porosity value), and the pressure drop almost remains constant in medium porosity (from 0.4 to 0.6). At the high porosity region (greater than 0.6), the pressure drop increases again. Figure 6 shows the effects of gas inlet stoichiometric ratios on the potential at the cathode/membrane interface. It seems that there is a common variation trend for the potential with different stoichiometric ratios. The catalyst layer potential is also very sensitive to the magnitude of porosity. When the porosity is about 0.4, the potential reaches a minimum value (the "minus" sign represents the potential direction). When the porosity is around 0.6, the corresponding potential is at the maximum. For the fixed flow rate at the inlet, smaller porosity results in a faster speed of reactants to the catalyst layer; however, the reactant might not be evenly distributed. At a higher porosity, reactants tend to distribute more uniformly but with lower speed, which causes a slow chemical reaction on the cathode side.

The effects of the GDL thickness are shown in Fig. 7. Figure 7 plots the average electrolyte fluid phase potential at the cathode/membrane interface with different values of GDL porosity for various GDL thicknesses. When the GDL thickness is 200 μm, the average potential is higher than the case of 300 μm. This result supports the fact that the cathode GDL performance is also governed by the action of product water, as proposed in literature [25]. A thinner GDL results in a larger oxygen transfer from the gas channel to the catalyst layer, and thus a larger potential is generated. However, a higher potential is accompanied by more water, which will transport back to the GDL and affects adversely the GDL pore performance. This study is beyond the scope of the present study, which may be implemented when a more thorough mathematical model is analyzed.

3 Statement of the Optimization Problem

As shown in the previous analysis, the parameters related to porous electrodes, such as the GDL porosity, permeability, and thickness, affect the performance of fuel cells. Some of these pa-

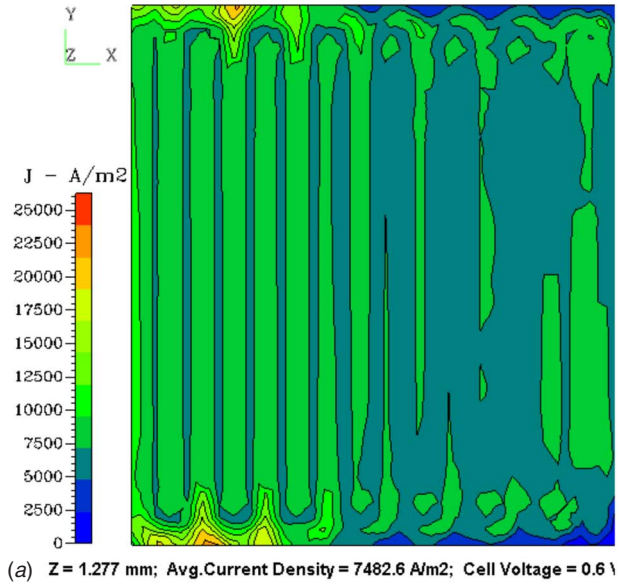

Fig. 12 Contours of current density over the membrane/cathode interface (*a*) before and (*b*) after optimization

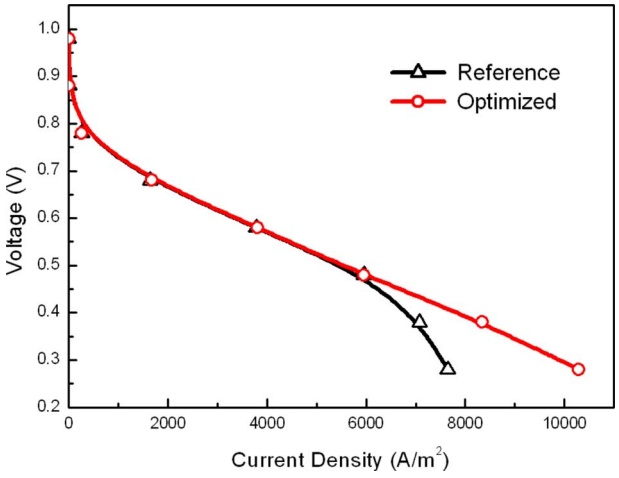

Fig. 13 Comparison of the polarization curve before and after the optimization

rameters, such as permeability and porosity, are controlled by the microstructure of the porous material. These parameters are mutually interdependent in a complex way. There must be an optimum parametric level at which the fuel cell has its best performance, which is the focus in the rest of this paper.

The optimization of a PEM fuel cell is classified into a multivariable constrained mix-programming problem. The objective function has the property of many extreme points and a Powell algorithm will be applied here.

3.1 Powell Algorithm. The Powell optimization algorithm is a multidimensional direct search method, which uses the function values only to determine an optimum solution. Figure 8 shows the searching scheme of the Powell method for a two-dimensional problem. Given an initial design configuration x^0, the algorithm starts by searching a set of conjugate directions, e_1, e_2, then e_1 again. The step sizes (i.e., the distance between x^0 and x_1^0) are optimally determined via a one-dimensional search. These three searches provide three design points from which a new direction is formed. The direction d^1, defined by $x_2^0 - x^0$, is conjugated to e_1 and e_2. In the next iteration, the direction e_1 is replaced by e_2, e_2 replaced by d^1, and another new conjugated direction is formed. The disadvantage of this Powell algorithm is that there is no guarantee that it will find the global fit-statistic minimum. The detailed description of the Powell algorithm can be found in Ref. [26].

3.2 Optimization Procedures. A multiparameter optimization is performed using a modularized program, which can alternate between the PEM fuel cell simulation and the numerical optimization. The program contains a main program based on the PYTHON code and three subroutine blocks for modeling, solving, and postprocessing. The initial values of the optimized parameters, including three electrode parameters and the inlet gas stoichiometric ratio, are shown in Table 3.

The numbers given within Table 3 correspond to the values of the parameters in the initial (reference) design of the PEM fuel cell. A higher potential loss is generated on the cathode side due to the slow kinetics of the oxygen reduction. The objective function of the optimization is to minimize the potential loss on the cathode side. Since the solid potential is assumed constant at the membrane/cathode interface, the objective function is then defined as the maximum potential of the electrolyte fluid phase at the membrane/cathode interface (at a cell voltage of 0.6 V), which is a measure of the activity degree of electrochemical reaction. A higher potential at the membrane/cathode interface corresponds to a more active electrochemical reaction and better cell performance.

Thus, the PEM fuel cell optimization problem can be defined as to maximize $\{-f[x(1),x(2),x(3),x(4),x(5),x(6),x(7),x(8)]\}$ with respect to $x(i)$, $i=1-8$, which corresponds to each variable shown in Table 3, respectively. This problem is subject to the following constraints:

$$5 \times 10^{-13}\ \text{m}^2 \leq x(1) \leq 5 \times 10^{-10}\ \text{m}^2$$

$$5 \times 10^{-13}\ \text{m}^2 \leq x(2) \leq 5 \times 10^{-10}\ \text{m}^2$$

$$0.1 \leq x(3) \leq 0.9$$

$$0.1 \leq x(4) \leq 0.9$$

$$0.2\ \text{mm} \leq x(5) \leq 0.5\ \text{mm}$$

$$0.2\ \text{mm} \leq x(6) \leq 0.5\ \text{mm}$$

$$x(7) = 1.5,\ 2,\ 2.5,\ 3,\ 4$$

$$x(8) = 1.3,\ 3$$

The upper and lower limits for each parameter are based on the study of Sec. 2.2.

3.3 Results and Discussions. Optimization results were obtained and shown in Table 4. The optimum values of the GDL permeability are slightly lower than the reference values; on the other hand, the optimum values of the GDL porosity are quite large compared to the initial values. Figure 9 displays the values of the objective function with iterations in the optimizing searching. The maximum potential of the electrolyte fluid phase at the membrane/cathode interface is 0.2704 V.

Figures 10–13 compare the performance of the fuel cell before and after the optimization. Figure 10 shows the oxygen mole fraction distributions in the GDL. Figure 11 shows the oxygen mole fraction distributions through the entire cathode thickness. Figures 10(*a*) and 11(*a*) show the reference results and Figs. 10(*b*) and 11(*b*) the results after the optimization. Three representative *X-Z* planes in Fig. 11 correspond to the fore cross plane, mid cross plane, and rear cross plane of the cathode side along the *Y* axial direction, respectively. By contrast, the average oxygen mole fraction in the optimized GDL is much higher, and thus more oxygen is brought to the cathode catalyst reaction site through the optimization. The major oxygen concentration gradients occur in the regions near the channel inlet or outlet. It is important to mention that the oxygen concentration distribution depends on the flow field design, which is a single-serpentine channel in this case.

Figure 12 displays the contour plots of the local current density over the membrane/cathode interface. Figure 12(*a*) shows the result for the reference case, where the values of the current density are inhomogeneous and lower than those after the optimization shown in Fig. 12(*b*). This is probably due to the oxygen mole fraction distribution denoted in Figs. 10 and 11. The current density in the membrane/cathode interface depends on the oxygen amount in the catalyst layer transported from the GDL. Clearly, after the optimization, the current density distributes more uniformly and its average

Figure 13 compares the polarization curves before and after the optimization. The line with circles represents the optimized results, which has a better performance in the mass limitation region (high current density). In this case, the concentration losses of the cell due to the oxygen transport limitation are decreased through the electrode's optimization. Thus, the chemical reaction should be stronger than the reference case since more oxygen is supplied for the high current density. However, for the low current density region, the cell voltage is not increased much due to the losses by the catalyst activation resistance and the membrane Ohmic resistance. These could be improved by including the optimization of the catalyst layer and the membrane in the model.

4 Conclusions and Future Work

A three-dimensional steady-state electrochemical mathematical model was established to study the performance of a PEM fuel cell. It is found that the pressure drop across the cathode GDL is influenced little by the changes of the gas inlet stoichiometric ratio. A relatively high potential occurs at a large permeability, which is due to the fact that more oxygen is transferred from the gas channel to the catalyst layer, resulting in a higher potential corresponding to a more active electrochemical reaction. Meanwhile, the effects of the thickness of the GDL on the average interface potential cannot be neglected since the cathode GDL performance is also governed by the action of water production.

Furthermore, the model is solved by the Powell multiparameter optimization algorithm. The optimum values of cathode/anode permeability, porosity, and thickness, and the stoichometric ratio are obtained. Through comparison with the reference case, the performance of a PEM fuel cell is improved after the optimization, especially at the high current density.

However, the Powell algorithm must be used cautiously since the obtained optimum value might not be the global maximum solution. The present work provides a computer-aided tool for designing future fuel cell engines with much higher power density and lower cost.

Acknowledgment

The authors would like to thank for the support of Oakland University Faculty Fellowship.

Nomenclature

A = area, m^2
c_f = concentration of fixed ionic in electrolyte, mol/m^3
C_p = specific heat at constant pressure, J/kg K
D = mass diffusivity of species, m^2/s
F = Faraday constant, 96,487 C/mol
i = current density, A/m^2
$\mathbf{i}$ = current density vector, A/m^2
l = thickness, m
k_p = hydraulic permeability, m^2
k_φ = electrokinetic permeability, m^2
M_i = molecular weight of species
n = electron number
p = pressure, Pa
R = gas constant, 8314 J/mol K
S = source term in governing equations or entropy, J/K
T = temperature, K
v = flow rate, m/s
$\mathbf{U}$ = velocity vector, m/s
x = mole fraction of species, mol/m^3
Y = mole fraction of species, mol/m^3
z_f = charge number

Greek Letters

α = Tafel constant
λ = heat conductivity, W/m K
Φ = phase potential, V
μ = viscosity, kg/m s
κ = permeability, m^2
σ = ionic conductivity, S/m
ρ = density, kg/m^3
ζ = stoichiometric ratio
ε = porosity
η_{act} = overpotential of activation, V

Subscripts

a = anode
c = cathode
e = electrolyte
i = species
m = continuity equation
ref = reference value
s = solid phase of electrode
u = momentum equation
φ = potential equation
eff = effective value

References

[1] Mathias, M., Roth, J., Fleming, J., and Lehnert, W., 2003, "Diffusion Media Materials and Characterization," *Handbook of Fuel Cells-fundamentals, Technology and Applications*, Vol. 3, Wiley, New York.
[2] Pharoah, J. G., 2005, "On the Permeability of Gas Diffusion Media Used in PEM Fuel Cells," J. Power Sources, **144**, pp. 77–82.
[3] Bernardi, D. M., 1991, "Mathematical Model of a Gas Diffusion Electrode Bonded to a Polymer Electrolyte," AIChE J., **37**, pp. 1151–1163.
[4] Springer, T. E., Zawodzinski, T. A., and Gottesfeld, S., 1991, "Polymer Electrolyte Fuel Cell Model," J. Electrochem. Soc., **138**, pp. 2334–2342.

[5] Yi, J. S., and Nguyen, T. V., 1998, "An Along-the-Channel Model for Proton Exchange Membrane Fuel Cells," J. Electrochem. Soc., **145**, pp. 1149–1159.
[6] Gurau, V., Liu, H. T., Kakac, S., 1998, "Two-Dimensional Model for Proton Exchange Membrane Fuel Cells," AIChE J., **44**, pp. 2410–2422.
[7] Yi, J. S., and Nguyen, T. V., 1999, "Multicomponent Transport in Porous Electrodes of Proton Exchange Membrane Fuel Cells Using the Interdigitated Gas Distributors," J. Electrochem. Soc., **146**, pp. 38–45.
[8] Um, S., Wang, C. Y., and Chen, K. S., 2000, "Computational Fluid Dynamics Modeling of Proton Exchange Membrane Fuel Cells," J. Electrochem. Soc., **147**, pp. 4485–4493.
[9] Dutta, S., Shimpalee, S., and Vanzee, J. W., 2000, "Three-Dimensional Numerical Simulation of Straight Channel Pem Fuel Cells," J. Appl. Electrochem., **30**, pp. 135–146.
[10] Natarajan, D., and Nguyen, T. V., 2003, "Three-Dimensional Effects of Liquid Water Flooding in the Cathode of a Pem Fuel Cell," J. Power Sources, **115**, pp. 66–80.
[11] Hwang, J. J., Chen, C. K., Savinell, R. F., Liu, C. C., and Wainright, J., 2004, "A Three Dimensional Numerical Simulation of the Transport Phenomena in the Cathodic Side of a PEMFC," J. Appl. Electrochem., **34**, pp. 217–224.
[12] Um, S., and Wang, C. Y., 2004, "Three-Dimensional Analysis of Transport and Electrochemical Reactions in Polymer Electrolyte Fuel Cells," J. Power Sources, **125**, pp. 40–51.
[13] Nguyen, P. T., Berning, T., and Djilali, N., 2004, "Computational Model of a Pem Fuel Cell With Serpentine Gas Flow Channels," J. Power Sources, **130**, pp. 149–157.
[14] Lum, K. W., and McGuirk, J. J., 2005, "Three-Dimensional Model of a Complete Polymer Electrolyte Membrane Fuel Cell—Model Formulation Validation and Parametric Studies," J. Power Sources, **143**, pp. 103–124.
[15] Ying, W., Sohn, Y.-J., Lee, W.-Y., Ke, J., and Kim, C.-S., 2005, "Three-Dimensional Modeling and Experimental Investigation for an Air-Breathing Polymer Electrolyte Membrane Fuel Cell (PEMFC)," J. Power Sources, **145**(2), pp. 563–571.
[16] Tuber, K., Pocza, D., and Hebling, C., 2003, "Visualization of Water Buildup in the Cathode of a Transparent Pem Fuel Cell," J. Power Sources, **124**, pp. 403–414.
[17] Chen, J. H., Matsuura, T., and Hori, M., 2004, "Novel Gas Diffusion Layer With Water Management Function for PEMFC," J. Power Sources, **131**, pp. 155–161.
[18] Hottinen, T., Noponen, M., Mennola, T., Himanen, O., Mikkola, M., and Lund, P., 2003, "Effect of Ambient Conditions on Performance and Current Distribution of a Polymer Electrolyte Membrane Fuel Cell," J. Appl. Electrochem., **34**, pp. 265–271.
[19] Williams, M. V., Kunz, H. R., and Fenton, J. M., 2004, "Operation of Nafion-Based PEM Fuel Cells With No External Humidification: Influence of Operating Conditions and Gas Diffusion Layers," J. Power Sources, **135**, pp. 122–134.
[20] Lee, H. K., Park, J. H., Kim, D. Y., and Lee, T. H., 2004, "A Study on the Characteristics of the Diffusion Layer Thickness and Porosity of the PEMFC," J. Power Sources, **131**, pp. 200–206.
[21] Grujicic, M., and Chittajallu, K. M., 2004, "Optimization of the Cathode Geometry in Polymer Electrolyte Membrane Fuel Cells," Chem. Eng. Sci., **59**, pp. 5883–5895.
[22] Patankar, S. V., 1980, "Numerical Heat Transfer and Fluid Flow," Hemisphere, New York.
[23] Pharoah, J. G., 2005, "On the Permeability of Gas Diffusion Media Used in PEM Fuel Cells," J. Power Sources, **144**, pp. 77–82.
[24] Um, S., Wang, C. Y., and Chen, K. S., 2000, "Computational Fluid Dynamics Modeling of Proton Exchange Membrane Fuel Cells," J. Electrochem. Soc., **147**, pp. 4485–4493.
[25] Chu, H.-S., Yeh, C., and Chen, F., 2003, "Effects of Porosity Change of Gas Diffuser on Performance of Proton Exchange Membrane Fuel Cell," J. Power Sources, **123**, pp. 1–9.
[26] Press, W. H., Flannery, B. P., Teukolsky, S. A., and Vetterling, W. T., 1986, "Numerical Recipes: The Art of Scientific Computing," Cambridge University Press, Cambridge, pp. 294–301.